Rheological interpretation of the structural change of LiB cathode slurry during the preparation process

Komoda, Yoshiyuki ; Ishibashi, Kaoru ; Kuratani, Kentaro ; Hidema, Ruri ; Suzuki, Hiroshi ; Kobayashi, Hironori

(Citation)
JCIS Open,5:100038

(Issue Date)
2022-04

(Resource Type)
journal article

(Version)
Version of Record

JCIS Open 5 (2022) 100038

Contents lists available at ScienceDirect

JCIS Open

journal homepage: www.journals.elsevier.com/jcis-open

Rheological interpretation of the structural change of LiB cathode slurry during the preparation process

Yoshiyuki Komoda [a,*], Kaoru Ishibashi [a], Kentaro Kuratani [b], Ruri Hidema [a], Hiroshi Suzuki [a], Hironori Kobayashi [b]

[a] Department of Chemical Science and Engineering, Graduate School of Engineering, Kobe University, 1-1, Rokkodai-chou, Nada-ku, Kobe, Hyogo, 657-8501, Japan
[b] Research Institute of Electrochemical Energy, Department of Energy and Environment, National Institute of Advanced Industrial Science and Technology (AIST), 1-8-31, Midorigaoka, Ikeda, Osaka, 563-8577, Japan

ARTICLE INFO

Keywords:
Krieger-Dougherty equation
Farris approach
Elastic modulus
AB network
Ball-milling effect
Bimodal slurry

ABSTRACT

The dispersion behavior of lithium cobalt oxide (LCO) and acetylene black (AB) particles in the preparation process of the cathode slurry of LiB is investigated from the rheological viewpoint. The cathode slurry is considered as the dispersion of coarse LCO particles in the viscoelastic AB slurry. Viscosity as well as loss modulus of the cathode slurry are estimated from those of the AB slurry using and compared the measured results. After forming the AB network structure or When AB content is high enough, LCO particles can enter and destroy the AB network structure. As a result, LCO particles and fragmented AB network structures are homogeneously mixed, exhibiting better discharge performance. Once the cathode slurry is excessively diluted, the LCO particles are excluded from the AB network structure, resulting in low discharge capacity. Over fragmentation using a high-shear device causes the AB network structure into too small segments, which also lowers the battery performance. Viscosity is helpful to understand the entrance of LCO particles into the AB network, and the storage modulus detects the destruction of the AB network structure during the preparation process of cathode slurry.

1. Introduction

To achieve a better and more sustainable future, establishing a cleaner and more efficient transportation system is urgently required. Electric vehicles (EVs) can replace fossil fuel use with renewable energy using rechargeable batteries. Although EVs nowadays become popular in some limited areas, we need to endeavor to acquire the manufacturing technology of high-performance rechargeable batteries toward the global spread of EVs. Lithium-ion Batteries (LiBs) are one the most popular rechargeable batteries these days. LiBs are composed of the cathode and anode, a separator, and electrolyte solution, which current collectors squeeze. Among them, active materials for the electrodes have attracted much attention because the capacity of the material directly contributes to the battery capacity. Although rare metal oxides are now basically used as active materials of the cathode, due to the enormous storage capacity of Lithium ions, Sulphur or its compounds are expected as the next-generation active materials for cathodes [1-7]. On the other hand, the anode contains carbon materials to store lithium ions. Due to the theoretical limit of the storage capacity, however, the active materials may shift to silicon-based materials [8–12]. When those traditional materials change into novel ones, manufacturing electrodes from raw materials will leave a practical problem [3–12].

The manufacturing process of electrodes consists of (1) dispersing particulate raw materials in a liquid phase to prepare an electrode slurry, (2) coating the slurry on a current collector, (3) drying the coated slurry, and (4) finally pressing the dried film. Among them, the preparation process of the slurry is the first step and significantly affects the following processes. In this decade, many researchers pointed out the significance of this process [13-21]. The effect of the preparation condition on the electrochemical performance has been demonstrated for the cathode systems of Sulphur-based materials [5,6] and Lithium oxide one [16-21]. For example, Lee et al. studied the effect of solvent addition and revealed the multi-step addition is favorable to obtain a fluid-like slurry. Kuratani et al. unveiled that excessive dispersion of such a fluid-like slurry resulted in a significant reduction in electrical conductivity and discharge capacity due to the destruction of the conductive network [19]. The importance of the slurry preparation process for better battery performance was proven in the slurries of anodes containing silicon [8] or

* Corresponding author. 1-1, Rokkodai-chou, Nada-ku, Kobe, Hyogo, 657-8501, Japan.
E-mail address: komoda@kobe-u.ac.jp (Y. Komoda).

https://doi.org/10.1016/j.jciso.2021.100038
Received 28 August 2021; Received in revised form 14 November 2021; Accepted 7 December 2021

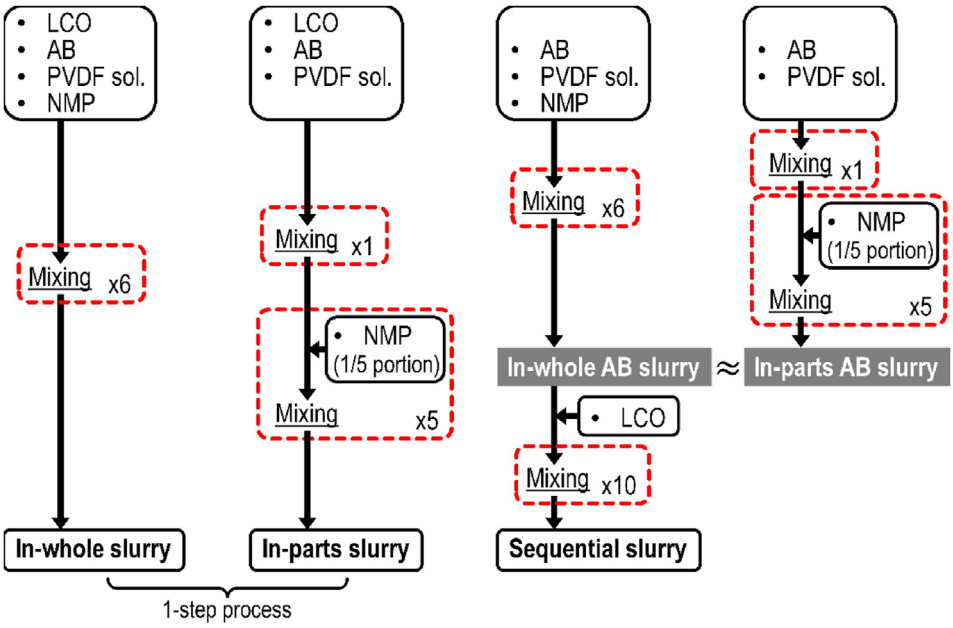

Fig. 1. Preparation scheme of cathode slurry.

carbon [22] particles. However, it is pointed out that the preparation process of cathode slurry is more difficult even in the choice of mixing equipment [23].

In the following processes after the slurry preparation, however, many unknown factors are affecting the final performance of the battery. For example, it is pointed out that a higher coating shear rate resulted in higher discharge capacity [24]. It is reported that the reduction of viscosity by elevating coating temperature improves the productivity of the cathode [25]. In most studies mentioned above, the rheological properties of the slurry were measured to characterize the slurries or to discuss the behavior of particulate materials and binders in the slurry [26-35]. Bauer and Notzel examined the determinant factors on the rheological behavior of the cathode slurry [27]. They depicted that finer particles control the rheological behavior. Ma et al. proposed the microstructure model to explain the rheological behavior of anode slurry, but the model for cathode slurry must be challenging [30]. The role of binder on the microstructure of cathode slurry has been studied from a rheological viewpoint [31]. Takeno et al. tried to understand the rheological behavior with the help of the impedance measurement [32,33]. The rheological characterization of cathode slurry has been utilized to clarify the microstructural change with the increase in particle content [34,35]. However, it seems that the way how the internal structure is developed during the slurry preparation process and the effect of the operating condition on the structure of the slurry have not been well studied for cathode slurry.

Our previous work focused on the slurry preparation step because the dispersion state of particulate raw materials in electrode slurry is to be controlled in this step and affects battery performance [19]. We demonstrated that the dispersion state was changed by the procedure of slurry preparation and characterized by viscoelastic properties. Additionally, those slurries were converted to electrodes respectively and exhibited different rate performances. It was brought to the light that gradual dilution of dense slurry gives a better dispersion state and better battery performance. It was also reported that excessive dispersion deteriorates rate performance, probably due to the destruction of electrically conductive paths, which is sensed by viscoelastic measurement even in the slurry. The cathode of LiBs contains a small number of conductive additives, i.e., acetylene black (AB), to construct the conductive paths. In other words, a scientific subject in the slurry preparation herein is the way how to attain a favorable dispersion state of particles even in the conflicting issues between the dispersion of AB particles and the maintenance of AB networks. For novel active materials, the performance gap between raw materials and finished batteries may be substantially caused by the lack of knowledge on the dispersion state of materials in the slurry. In the present study, we again focus on the rheological properties of the slurry to understand the internal structure in terms of its formation or destruction during the slurry preparation process and then investigate the effect of mixing procedures on the structural change.

2. Experiment

2.1. Materials and slurry preparation

The cathode slurry prepared in the present study consists of lithium cobalt oxide ($LiCoO_2$ or LCO, Nippon Chemical Industrial Co., Ltd., Japan) as active materials, acetylene black (AB, Li-100, Denka Co., Ltd., Japan) as conductive aids, polyvinylidene fluoride (PVDF, #1120, $M_W = 2.8 \times 10^5$, Kureha Co., Ltd., Japan) as a binder, and N-methyl-2-pyrrolidone (NMP, FUJIFILM Wako Pure Chemical Co., Ltd.) as a solvent. PVDF is added as 12 wt% NMP solution and then finally diluted to 8 wt% with the addition of NMP. Mean particle sizes of LCO and AB are 6.8 μm and 35 nm, and their specific gravities are 5.1 and 2.0, respectively. However, AB particles often form aggregates, which is difficult to disaggregate. AB particles were dispersed into a plenty amount of NMP and then a single aggregate was observed by SEM after evaporating NMP. As a result, we found that the aggregate has a size of roughly 500 nm. The cathode slurry in the present study can be considered a mixture of 0.5 μm AB aggregates, 6.8 μm LCO particles, 12 wt% PVDF solution.

Different procedures produce three kinds of cathode slurries, as shown in Fig. 1. According to a practical slurry preparation procedure, all materials other than diluent NMP are first mixed in a 150 ml cup, and then the addition of 1/5 portion of diluent NMP and the mixing are repeated five times. Each mixing operation is carried out using a planetary centrifugal mixer (ARE-310, Thinky Co., Ltd., Japan) operated at 2000 rpm for 3 min in each. As a labor-saving simple procedure, all materials are added to the cup at one time and then mixed six times in total. They are referred to as “in-whole” and “in-parts” processes hereafter. On the contrary, to disperse each material carefully in separate stages, AB slurry is first prepared using all materials other than LCO either by in-whole or in-parts process. Then, since they showed similar

Table 1
Compositions of test slurries.

	Cathode slurry		LCO slurry	AB slurry
	Weight ratio	Vol. %		
LCO	100	19	20	–
AB	4	2	–	2.5
PVDF	6.5	79	80	97.5
NMP	75			

rheological behavior, LCO particles were added to the in-whole AB slurry, and the mixing operation was repeated additional ten times. The procedure is called a "sequential process" hereafter.

The composition of the cathode slurry is represented by the weight fractions of AB and PVDF with respect to LCO. The amount of diluent NMP was decided to reduce the concentration of the PVDF solution from 12 to 8 wt%. To characterize the dispersion state of LCO particles in PVDF solution, LCO slurry is prepared using all materials except AB. The composition of the cathode slurry in detail is found in Table 1 and that of AB or LCO slurry. The cathode slurry with higher AB content is too elastic, exhibiting poor fluidity, whereas enough AB network structure cannot be formed in the cathode slurry containing less AB.

2.2. Rheological measurements of cathode slurries

Rheological measurements are performed at 25 °C using a stress-controlled rheometer (MCR702, Anton Paar GmbH, Austria) with a cone-plate geometry having a diameter of 50 mm and a cone angle of 1°. In the viscosity measurement, the pre-shear of 0.1 s^{-1} for 200 s first applies to the sample for good reproducibility, and then the shear rate increases logarithmically from 0.1 to 1000 s^{-1}. Viscosity at each shear rate is obtained after attaining stable shear stress. In the viscoelastic measurement, on the other hand, storage and loss moduli are measured as increasing the frequency logarithmically from 0.1 to 100 Hz at the maximum strain of 0.01%, being known as a frequency sweep test. When the maximum strain is sufficiently small, the internal structure of the slurry is maintained during this measurement. Storage modulus stands for the stiffness or elasticity of the structure formed in the slurry, whereas loss modulus corresponds to fluidity. Loss tangent is the ratio of loss modulus to storage one.

3. Results and discussion

3.1. Estimation of rheological properties of cathode slurry

Various equations to estimate the viscosity of a suspension of coarse non-colloidal particles η are proposed using particle volume fraction φ and dispersing medium viscosity η_0, such as the classical Krieger-Dougherty (K-D) equation as shown in Eq. (1) [36].

$$\eta = \eta_0 \left(1 - \frac{\varphi}{\varphi_m}\right)^{-2.5\varphi_m} \quad (1)$$

where φ_m indicates the maximum volume fraction of the particles. The dispersing medium is treated as a continuum if its internal microstructure is sufficiently smaller than the particle. Lutringer and Weill investigated the gyration size of PVDF molecules in various solvents by light scattering technique [37]. Since the PVDF used in this study is KF1100, which should exhibit properties similar to KF1000 found in the reference, the size of PVDF used is estimated to be approximately 30 nm, which is much smaller than the size of AB aggregate. Therefore, the PVDF solution is considered a homogenous dispersing medium. Similarly, since AB aggregates are sufficiently smaller than a single LCO particle, the mixture of AB particles and PVDF solution is still considered as a homogenous dispersing medium of coarse LCO particles in the cathode slurry. According to Farris approach [38], we can calculate the cathode slurry viscosity using the volume fraction of coarse LCO particles, φ_L and AB slurry viscosity, η_{AB}. The AB slurry viscosity is calculated using the solid volume fraction in AB slurry, φ^f_{AB} and the PVDF solution viscosity, η_P. When applying the K-D equation, the cathode slurry viscosity is expressed by Eq. (2). The effective maximum volume fractions $\varphi^f_{m,AB}$ and $\varphi_{m,L}$ are introduced here to consider the difference in the packing state of each particle due to the formation of aggregates.

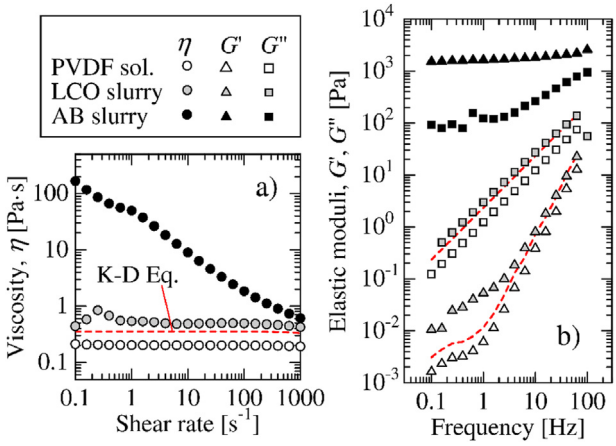

Fig. 2. Rheological properties of PVDF solution, AB slurry, and LCO slurry. "K-D Eq." represents the estimated value of LCO slurry from the rheological properties of PVDF solution and particle volume fraction of LCO particles using Krieger-Dougherty Equation.

$$\eta_{cathode} = \eta_{AB}\left(1 - \frac{\varphi_L}{\varphi_{m,L}}\right)^{-2.5\varphi_{m,L}} = \eta_P\left(1 - \frac{\varphi^f_{AB}}{\varphi^f_{m,AB}}\right)^{-2.5\varphi^f_{m,AB}}\left(1 - \frac{\varphi_L}{\varphi_{m,L}}\right)^{-2.5\varphi_{m,L}} \quad (2)$$

To elucidate the effect of particle aggregation on the cathode slurry viscosity, the rheological behaviors of the PVDF solution, AB slurry, and LCO slurry are examined. 8 wt% PVDF solution is prepared by the addition of NMP to 12 wt% PVDF solution, and the viscosity, η_P, is measured. LCO or AB particles are dispersed into the 8 wt% PVDF solution by the in-whole process to produce LCO or AB slurry, respectively. As already given in Table 1, the particle volume fractions of the LCO and AB slurries were $\varphi^c_L = 0.20$ and $\varphi^f_{AB} = 0.025$, respectively. The results of the viscosity measurement are shown in Fig. 2 together with those of the frequency sweep test. PVDF solution is considered a Newtonian fluid, exhibiting constant viscosity, linear relationship of loss modulus against frequency, and loss modulus sufficiently larger than storage one. In general, when polymer chains entangle each other in the solution, the dissociation of the entanglement with the increase in shear rate results in viscosity decreases. Therefore, it is found that PVDF molecules possess relatively small volumes and are separated from each other. Moreover, the rheological behaviors of the LCO slurry and PVDF solution are alike. The LCO slurry viscosity calculated by the K-D equation using η_P, φ^c_L and the maximum volume fraction $\varphi^c_{m,L} = 0.64$, is expressed by a dashed red line in Fig. 2a. Dynamic moduli are also multiplied by the same degree of viscosity increase and expressed as dashed red lines in Fig. 2b as well. The good agreements between measured and estimated values in either viscosity or dynamic moduli suggest that LCO particles are well dispersed in the PVDF solution. Meins et al. studied the effect of particle addition into polymer melt on dynamic moduli [39]. They insisted that the frequency-dependence of liner elastic moduli did not change with the inclusion of micron-sized particles because large solids only play the role of increasing hydrodynamic perturbations or viscous terms.

In contrast, the AB slurry viscosity is noticeably large and decreases significantly as increasing shear rate. Even at the highest shear rate of 1000 s^{-1}, the relative viscosity η_{AB}/η_P is 3.5, which corresponds to the

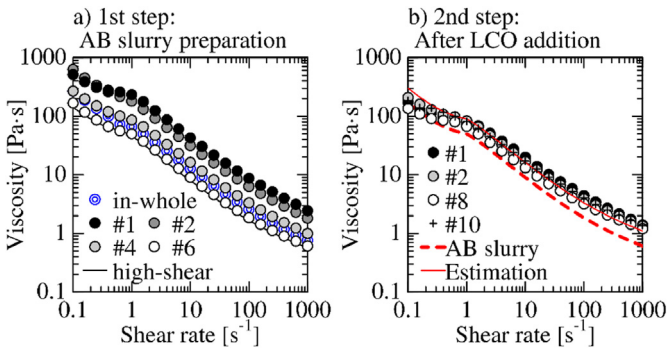

Fig. 3. Viscosity changes in the first and second steps of the sequential preparation process. AB slurry is finally obtained in the first step, while the second step produces cathode slurry. The cathode slurry viscosity is estimated from AB slurry viscosity and LCO volume fraction and denoted by "Estimation."

particle volume fraction of 0.35 in the K-D equation. The storage modulus is much larger than the loss modulus and roughly constant in the entire frequency range. The plateau region of storage modulus in a low-frequency range, namely a second plateau, indicates the presence of the network structure of AB aggregates that extends throughout the slurry. It is thus concluded that an effective solid volume fraction is increased not only by the aggregation of primary AB particles but also by the network formation of AB aggregates and gradually decreased with the structural destruction as increasing shear rate, which is the mechanism to exhibit the shear-thinning behavior. The following insight can be drawn from these rheological examinations; LCO particles are essentially easy to be dispersed into PVDF solution; the scientific subjects in the slurry preparation process are how LCO particles and AB network structures are homogenized and how the stiff AB network structure is destructed.

Before moving to the rheological analysis of the slurry preparation process, the role of PVDF in cathode slurry is discussed. When AB particles are dispersed into NMP without PVDF, the viscosity and elastic moduli of the slurry are in the same order as AB slurry containing PVDF. However, PVDF/NMP solution exhibits roughly 100 times larger viscosity compared to NMP. Therefore, AB particles form a significantly large network structure in NMP without PVDF, showing a drastic viscosity increase. In other words, the PVDF molecule adsorbs on the surface of AB aggregates and has a role in suppressing the excessive growth of the AB network structure.

3.2. Rheological analysis of sequential preparation process

Our previous work on cathode slurry reported that the in-parts process could produce an electrode exhibiting better rate performance. Although the control of the dispersion state of AB particles must be a crucial factor to obtain better cathode slurry, the process affecting the formation of the AB network structure has not been identified. Firstly, a cathode slurry is prepared by the sequential process consisting of two steps; the preparation of AB slurry and the dispersion of LCO particles into the AB slurry. In the first step, the AB slurry is prepared by the in-whole or in-parts process. After the addition of LCO particles into the AB slurry, the mixing of the mixture is repeated in the second step. The effect of the repetition of mixing on the internal structure change is examined in each step.

3.2.1. Viscosity change

Fig. 3 summarizes the viscosity changes of the AB slurry in the first step and the cathode slurry in the second step. In these figures, *#n* stands for the result after the *n*-th mixing operation. In Fig. 3a presenting the viscosity change of AB slurry prepared by the in-parts process, #1 corresponds to before the first addition of diluent NMP. Alternatively, #6 means the AB slurry after the final addition of NMP and is referred to as

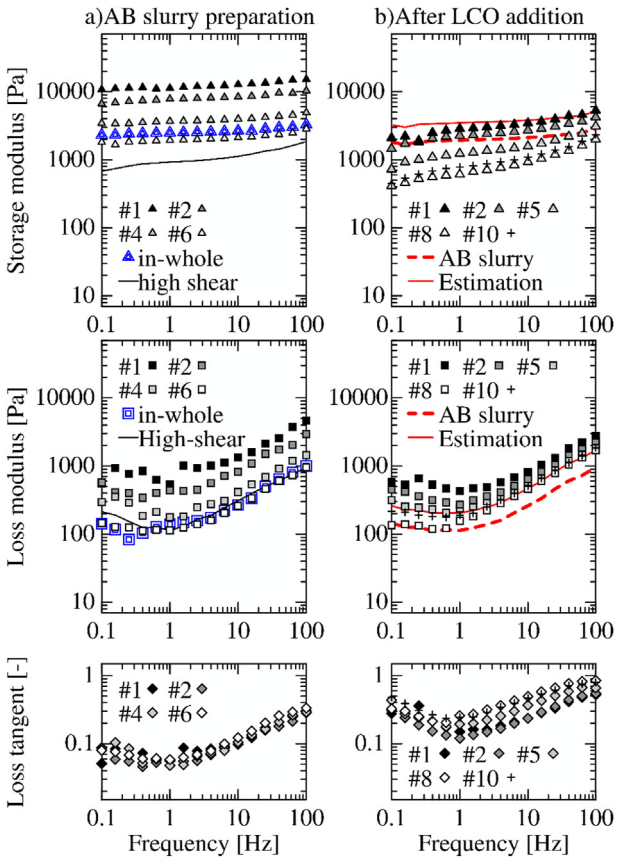

Fig. 4. Viscoelastic behavior of the cathode slurry in the sequential process. "*#n*" indicates the result after *n*th cycle of the mixing operation.

the in-parts AB slurry. In contrast, since the viscosity of the in-whole AB slurry did not show any significant change regardless of the repetition of mixing, the result after the final mixing operation is plotted as double blue circles. The in-parts AB slurry after being subjected to high-shear is shown as a solid curve as well. The high shear was applied using Filmix, in which a rotor can rotate at the tip speed of 40 m/s in a stationary vessel. Since the slurry is sheared in a gap of 5 mm, the applied shear rate is estimated to be 2000 s^{-1}. The detail of this experiment is available in our previous publication [19]. The gradual decrease of the viscosity of the in-parts AB slurry is largely due to the dilution by NMP. Since the shape of the viscosity curve was almost the same despite the progress of mixing, the internal structure of the AB slurry did not change during the in-parts process. Additionally, the viscosity of the in-parts AB slurry finally coincided with that of the in-whole AB slurry and could not be reduced further by the high-shear mixing device. Therefore, it was proven that the internal structure of AB slurry is difficult to control by the repetition of mixing or the application of high shear as far as investigated.

In the second step, LCO particles are added to the in-parts AB slurry, and the mixing operation using the same planetary centrifugal mixer is repeated ten more times. The viscosities of the AB slurry containing LCO particles, which is a cathode slurry, during this step are shown in Fig. 3b. Regardless of the repetition of mixing, no significant viscosity change is observed in this step. A dashed red curve in Fig. 3b indicates the result of the in-parts AB slurry. Assuming that the cathode slurry is the mixture of completely dispersed LCO particles and the in-parts AB slurry, the viscosity of the cathode slurry is estimated by the K-D equation using the AB slurry viscosity, η_{AB} and LCO volume fraction, ($\varphi_L = 0.19$), and expressed by a solid red curve as well. The viscosity of the cathode slurry is between the AB slurry and the estimated values at the shear rates less than 1 s^{-1}, but it agrees well with the estimation at higher shear rates. In general, the viscosity decreasing trend flattens out when the destruction of the

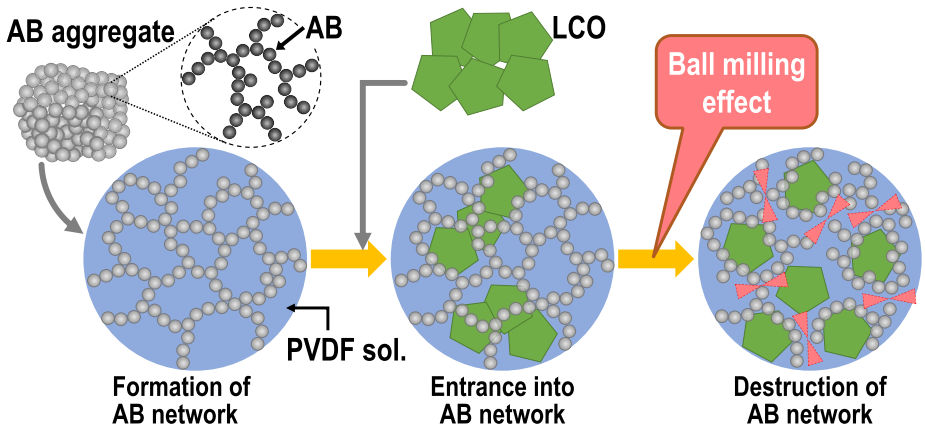

Fig. 5. Internal structure change in the sequential process.

internal structure is completed, and then a stable state is attained at the shear rate range. The slope change around the critical shear rate manifests the transition in the scale of the AB network structure to be destructed. Under moderate shear flow, since LCO particles are embedded in the huge AB network structure, the volume effect of LCO particles on the cathode slurry viscosity is considered to be limited. Above the critical shear rate, however, the AB network structure is largely broken up into smaller network segments, and the volumetric or hydrodynamic effect of LCO particles on the viscosity fully shows up.

3.2.2. *Viscoelastic analysis*

Viscosity measurement indicates that a higher-order AB network structure remains at lower shear rates, and the elasticity caused by the structure considerably affects shear stress. However, the internal structure is destructed during the viscosity measurement because a slurry is subjected to shear flow for a long time, even at a meager shear rate. Therefore, viscoelastic properties under sufficiently small deformation, known as a linear viscoelastic regime, are more suitable to detect the change of the structure. Fig. 4 summarizes the changes of the frequency dependences of the storage and loss moduli of the in-parts AB slurry in the first step and the cathode slurry in the second step. In the AB slurry preparation step (Fig. 4a), both elastic moduli gradually decrease with the addition of NMP and coincide with those of the in-whole AB slurry after the final mixing operation. These results qualitatively agree well with the behavior of the viscosity change. Additionally, no significant change in frequency dependency is observed for both elastic moduli. To neglect the effect of dilution by NMP, the ratio of loss modulus to storage one, being a loss tangent, is plotted in the bottom figure. No remarkable change in the loss tangent besides the repetition of mixing in the entire frequency range indicates that the internal structure of AB slurry does not change in this step. This figure also indicates that the high-shear mixing solely reduces storage modulus despite no obvious change in loss modulus.

In the second step or after LCO addition, it was unveiled that storage and loss moduli change differently, as seen in Fig. 4b. Dashed and solid red curves in this figure represent the elastic moduli of the in-parts AB slurry and the cathode slurry estimated by the K-D equation, respectively. After the first mixing operation, the storage modulus is slightly larger than the AB slurry but smaller than the estimation, while the loss modulus increases roughly four times and is much larger than the estimation. It means that the AB slurry still dominates the storage modulus of the cathode slurry, but the increase in solid volume fraction by LCO addition is insufficient to explain the loss modulus increase. Therefore, it is deduced that LCO particles still form aggregates to increase effective volume fraction and do not yet destroy the AB network. As the mixing operation is repeated, the storage modulus gradually decreases and becomes smaller than the AB slurry. Thus, the fact indicates that the mixing with LCO particles significantly destructs the AB network structure up to

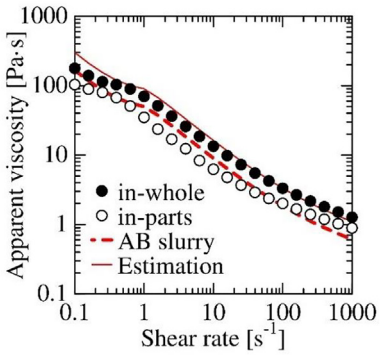

Fig. 6. Viscosity of cathode slurry prepared by in-whole or in-parts process.

the 8th operation. It is presumed that large and heavy LCO particles play roles in destroying the AB network structure, as can be seen in a ball-milling process. No further significant change in storage modulus after the 9th operation suggests that the stable dispersion state is obtained after the 8th.

On the contrary, after the 5th operation, loss modulus agrees well with the estimation at frequencies higher than 10 Hz but stays between the AB slurry and estimated value at lower frequencies. Thus, the behavior of loss modulus resembles that of the viscosity and can be explained similarly. That is, shear stress against slow deformation is caused largely by the elasticity of the AB network structure, whereas the effective solid volume fraction increases the shear stress under quick oscillation. Fig. 5 illustrates the internal structure change predicted by the rheological analysis in the sequential process. When the network structure of AB aggregates is developed entirely in the slurry, LCO particles can enter and destroy the structure by the ball-milling effect. As a result, the connection of AB aggregates is broken up, and the network structure is segmented, but the sum of the effective volume of the network structure is rarely changed.

3.3. *Rheological characterization of the 1-step preparation process*

We revisit our finding that the cathode produced using in-whole slurry showed a low rate performance rather than that from in-parts slurry [19]. In the manufacturing process of the electrode, the slurry was applied slowly over an aluminum foil to minimize the structure change by the shear application and then dried up on the hot plate maintained at 60 °C, at which the materials are distributed uniformly due to no sedimentation of LCO particles and the networking of AB aggregates. Therefore, the difference in the network structure of AB aggregates caused by the slurry preparation process is the dominant factor in the rate

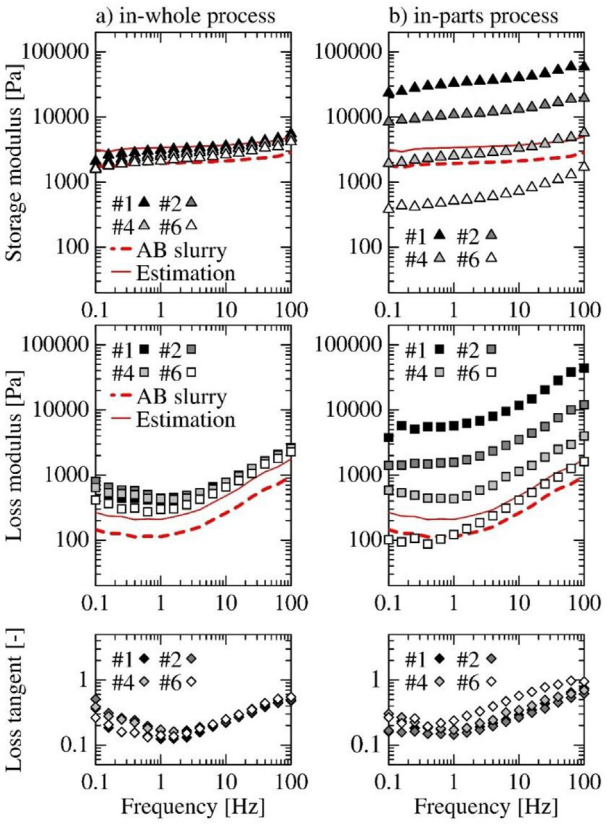

Fig. 7. Elastic moduli of cathode slurry prepared by in-whole or in-parts process.

performance. Therefore, we concluded this is caused by the insufficient formation of the electrically conductive pathways, which was confirmed by the electrical conductivity and X-ray CT images of the electrodes and by the viscoelastic properties of the slurries. In the latter part of this study, the origin of the disadvantage of the "labor-saving" in-whole process is depicted while contrasting it with the "practical" in-parts process.

3.3.1. *Viscosity of in-parts and in-whole cathode slurries*

The viscosities of the cathode slurry prepared by in-parts or in-whole process are plotted in Fig. 6 together with those of the in-parts AB slurry and the cathode slurry estimation in a similar manner to Fig. 3. The viscosity of the in-whole cathode slurry is reasonably predicted using the AB slurry viscosity and LCO volume fraction. This result indicates that the AB network structure in the cathode slurry is equivalent to that in the in-parts AB slurry and most LCO particles locate outside the AB network structure. In contrast, the in-parts cathode slurry and AB slurry exhibit approximately the same viscosities in the entire shear rate range, although the cathode slurry is a mixture of the AB slurry and 19 vol% of LCO particles. In the lower shear rate range less than 1 s^{-1}, this can be explained by embedding LCO particles in a higher-order AB network structure. The AB network structure is fractured at higher shear rates, and the hydrodynamic effects of LCO particles should emerge. Therefore, the dispersing medium of LCO particles in the in-parts cathode slurry is less viscous than the in-parts AB slurry. In other words, it was proven that the dispersion of AB particles is progressed during the in-parts process with the coexistence of LCO particles.

3.3.2. *Viscoelastic differences between the in-parts and in-whole cathode slurries*

To reveal the internal structure change in each slurry preparation process, the frequency sweep test of cathode slurries is shown in Fig. 7, similarly to the sequential cathode slurry. These figures include the results of the in-parts AB slurry and the cathode slurry estimation as references. For the in-whole slurry (Fig. 7a), both elastic moduli slightly decreased with the repetition of mixing operations. Furthermore, the storage modulus eventually coincides with the in-parts AB slurry, while the loss modulus agrees well with the estimation in the entire frequency range. Since the AB network causes the elasticity, it is considered that equivalent AB network structures are formed in the in-whole cathode slurry and the in-parts AB slurry. LCO particles outside the AB network structure increase the effective volume fraction so that the loss modulus solely increases. A stable loss tangent also suggests no structural change related to AB network structure. All these findings perfectly support the discussion based on viscosity measurement. Therefore, it is concluded that the ball-milling effect of LCO particles cannot be expected in the in-whole process, presumably due to the considerable surface distance of LCO particles.

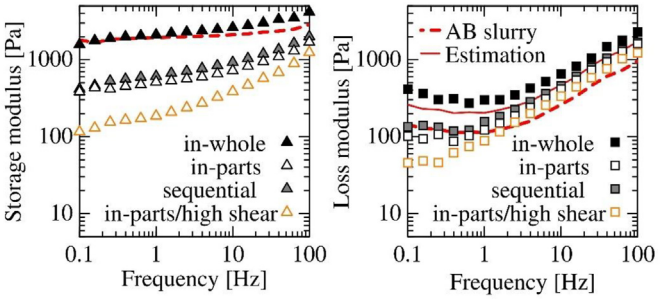

Fig. 8. Viscoelastic comparison among cathode slurries prepared different processes.

During the in-parts process, the formation of AB network structure, the destruction, and the dilution by NMP are taken place simultaneously. Consequently, either elastic modulus is decreased drastically as the progress of mixing, as shown in Fig. 7b. The storage modulus eventually becomes much smaller than the AB slurry, while the loss modulus falls between the AB slurry and estimation. The elastic moduli of AB slurry were decreased to 1/10 by the addition of NMP, as shown in Fig. 4a, whereas the cathode slurry decreased the elastic moduli to 1/100. The result evidences the destruction of the AB network structure during the in-part process. Paying attention to the frequency dependence of loss tangent to neglect the difference in volume fraction, the noticeable improvement of fluidity at a frequency more than 1 Hz appears at the 6th. The fact implies that dense slurry mixing and more than six repetitions of mixing operations are required to obtain the cathode slurry producing better performance. The optimization of the initial particle volume fraction and the repetition of the mixing operation is out of the objective of the present study but should be conducted in future studies.

3.3.3. *Effect of high-shear mixing on the internal structure*

The final section compares the frequency sweep tests of the final cathode slurries prepared by different processes, as shown in Fig. 8. The in-parts slurry further dispersed using the high-shear mixing device is expressed as "in-parts/high shear." The detail of the shearing device has already been explained in section 3.2.1. Firstly, it can be found that the sequential and in-parts processes produced the slurry exhibiting the same rheological behavior. Therefore, it is suggested that the stepwise dispersion of AB and LCO particles into PVDF solution until obtaining stable rheological properties at each step is acceptable for obtaining favorable cathode slurry, without dense slurry mixing and gradual dilution.

After being subjected to high shear, the storage modulus of the cathode slurry can be further reduced in the entire frequency range. Therefore, high shear flow could destroy the AB network structure into smaller segments, and an effective solid volume fraction would be somewhat reduced. The reduction in the effective solid volume fraction

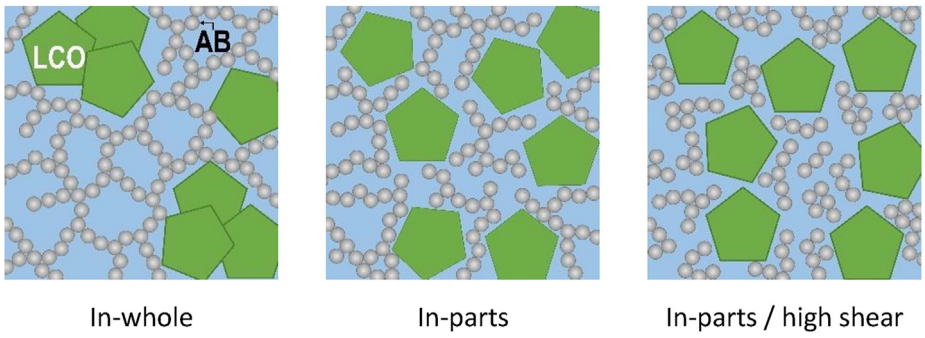

Fig. 9. Internal structure of cathode slurries prepared by different processes. It is difficult even for LCO particles to disperse in the less condensed slurry containing excessively large network structures of AB, while a high-shear mixing device may split AB network structure into too small pieces to keep electrically conductive pass.

relates to the slight decrease in loss moduli at high frequencies, whereas a remarkable reduction at low frequencies is due to the significant destruction of the AB network structure. Consequently, the in-parts/high shear cathode slurry contains the excessively fragmented AB network structures, which are too small to form electrically conductive pathways in the electrode during drying. Fig. 9 shows an illustration of the difference in the internal structure among these cathode slurries.

4. Conclusions

The change of the internal structure of the cathode slurry composed of coarse LCO and fine aggregates of AB particles in different preparation procedures was investigated from a rheological viewpoint. LCO particles are readily dispersed into PVDF solution, but it was found that the network structure of AB aggregates in PVDF solution is tough enough not to be destructed as far as using a planetary centrifugal mixer. Assumed that the cathode slurry is the mixture of complete dispersed LCO particles and viscoelastic AB slurry, the rheological behavior of the cathode slurry could be estimated by Krieger-Dougherty equation. This estimation is also applied for loss modulus and used to evaluate the state of AB network structure in cathode slurry. When the AB slurry is dispersed with LCO particles, it is revealed that LCO particles enter and destroy the AB network structure. A similar fragmentation of AB network structure was conducted when dense cathode slurry is first prepared and then gradually diluted by solvent. On the other hand, in the cathode slurry initially diluted, LCO particles could not enter and destroy the AB network structure. Moreover, a high-shear mixing device excessively destroyed the AB network into much smaller segments, which may be too dispersed to form the percolation of AB particles during drying. The comparison of viscosity between the cathode and AB slurries is helpful to detect the entrance of LCO particles into the AB network and the release from the structure under higher shear rates. Loss modulus and viscosity provide similar information, while the formation of a higher-order structure of the AB network and its destruction could be characterized only by the frequency sweep test of storage modulus.

Funding

This research did not receive any specific grant from funding agencies in the public, commercial, or not-for-profit sectors.

Declaration of competing interests

The authors declare that they have no known competing financial interests or personal relationships that could have appeared to influence the work reported in this paper.

Acknowledgments

This study was carried out under AIST-Kobe university cross-appointment framework. The corresponding authors thank the opportunity initiated by both organizations.

References

[1] J.B. Goodenough, K.S. Park, The Li-ion rechargeable battery: a perspective, J. Am. Chem. Soc. 135 (4) (2013) 1167–1176.
[2] A. Manthiram, Y. Fu, S.H. Chung, C. Zu, Y.S. Su, Rechargeable lithium–sulfur batteries, Chem. Rev. 114 (23) (2014) 11751–11787.
[3] J. Fang, F. Qin, J. Li, K. Zhang, W. Liu, M. Wang, F. Yu, L. Zhang, Improved performance of sulfur cathode by an easy and scale-up coating strategy, J. Power Sources 297 (2015) 265–270.
[4] D. Lv, J. Zheng, Q. Li, X. Xie, S. Ferrara, Z. Nie, L.B. Mehdi, N.D. Browning, J.G. Zhang, G.L. Graff, J. Liu, J. Xiao, High energy density lithium–sulfur batteries: challenges of thick sulfur cathodes, J. Adv. Energy Mater. 5 (2015) 1402290.
[5] S. Waluś, A. Robba, R. Bouchet, C. Barchasz, F. Alloin, Influence of the binder and preparation process on the positive electrode electrochemical response and Li/S system performances, Electrochim. Acta 210 (2016) 492–501.
[6] P. Titscher, P. Schön, M. Horst, U. Krewer, A. Kwade, Increasing energy densities of sulfur cathodes using dispersing and calendering processes for lithium–sulfur batteries, Energy Technol. 6 (2018) 1139–1147.
[7] O.O. Kapitanova, K.V. Mironovich, D.E. Melezhenko, V.V. Rokosovina, S.Y. Ryzhenkova, S.V. Korneev, T.B. Shatalova, C. Xu, F.S. Napolskiy, D.M. Itkis, V.A. Krivchenko, Modified carbon nanotubes for water-based cathode slurries for lithium–sulfur batteries, J. Mater. Res. 34 (2019) 634–641.
[8] B.P.N. Nguyen, S. Chazelle, M. Cerbelaud, W. Porcher, B. Lestriez, Manufacturing of industry-relevant silicon negative composite electrodes for lithium ion-cells, J. Power Sources 262 (2014) 112–122.
[9] L. Zhang, Y. Liu, B. Key, S.E. Trask, Z. Yang, W. Lu, Silicon nanoparticles: stability in aqueous slurries and the optimization of the oxide layer thickness for optimal electrochemical performance, ACS Appl. Mater. Interfaces 9 (2017) 32727–32736.
[10] Z. Karkar, D. Guyomard, L. Roué, B. Lestriez, A comparative study of polyacrylic acid (PAA) and carboxymethyl cellulose (CMC) binders for Si-based electrodes, Electrochim. Acta 258 (2017) 453–466.
[11] L.H. Huang, C.C. Li, Effects of interactions between binders and different-sized silicons on dispersion homogeneity of anodes and electrochemistry of lithium-silicon batteries, J. Power Sources 409 (2019) 38–47.
[12] G. Park, M.J. Ji, S.H. Jung, B.K. Ju, B.H. Choi, Effects of adding HPC to Si-alloy anode slurry of lithium secondary battery, J. Electrochem. Soc. 162 (2015) A488–A492.
[13] V. Wenzel, H. Nirschl, D. Nötzel, Influence of dry mixing and distribution of conductive additives in cathodes for lithium ion batteries, Energy Technol. 3 (2015) 692–698.
[14] A. Kraytsberg, Y. Ein-Eli, Conveying advanced Li-ion battery materials into practice the impact of electrode slurry preparation skills, Adv. Energy Mater. 6 (2016) 1600655.
[15] G.W. Lee, J.H. Ryu, W. Han, K.H. Ahn, S.M. Oh, Effect of slurry preparation process on electrochemical performances of LiCoO2 composite electrode, J. Power Sources 195 (2010) 6049–6054.
[16] W. Zhang, X. He, W. Pu, J. Li, C. Wan, Effect of slurry preparation and dispersion on electrochemical performances of LiFePO 4 composite electrode, Ionics 17 (2011) 473–477.
[17] A. Ponrouch, M.R. Palacín, On the impact of the slurry mixing procedure in the electrochemical performance of composite electrodes for Li-ion batteries: a case study for mesocarbon microbeads (MCMB) graphite and Co3O4, J. Power Sources 196 (2011) 9682–9688.
[18] Y.I. Kwon, J.D. Kim, Y.S. Song, Agitation effect on the rheological behavior of lithium-ion battery slurries, J. Electro. Mater. 44 (2015) 475–481.
[19] K. Kuratani, K. Ishibashi, Y. Komoda, R. Hidema, H. Suzuki, H. Kobayashi, Controlling of dispersion state of particles in slurry and electrochemical properties of electrodes, J. Electrochem. Soc. 166 (4) (2019) A501–506.
[20] M. Wang, D. Dang, A. Meyer, R. Arsenault, Y.T. Cheng, Effects of the mixing sequence on making lithium ion battery electrodes, J. Electrochem. Soc. 167 (10) (2020) 100518.

[21] K. Konda, S.B. Moodakare, P.L. Kumar, M. Battabyal, J.R. Seth, V.A. Juvekar, R. Gopalan, Comprehensive effort on electrode slurry preparation for better electrochemical performance of LiFePO4 battery, J. Power Sources 480 (2020) 228837.
[22] Y. Komoda, Y. Chizaki, H. Suzuki, R. Hidema, Viscoelastic analysis of dispersion process of highly concentrated suspension, J. Soc. Powder Technol. Japan 53 (2016) 371–379 (in Japanese).
[23] D. Liu, L.-C. Chen, T.-J. Liu, T. Fan, E.-Y. Tsou, C. Tiu, An effective mixing for lithium ion battery slurries, Adv. Chem. Eng. Sci. 4 (4) (2014) 50729.
[24] R.M. Saraka, S.L. Morelly, M.H. Tang, N.J. Alvarez, Correlating processing conditions to short-and long-range order in coating and drying lithium-ion batteries, ACS Appl. Energy Mater. 3 (12) (2020) 11681–11689.
[25] W.B. Hawley, J. Li, Electrode manufacturing for lithium-ion batteries—analysis of current and next generation processing, J. Energy Storage 26 (2019) 100994.
[26] K.Y. Cho, Y.I. Kwon, J.R. Youn, Y.S. Song, Evaluation of slurry characteristics for rechargeable lithium-ion batteries, Mater. Res. Bull. 48 (2013) 2922–2926.
[27] W. Bauer, D. Nötzel, Rheological properties and stability of NMP based cathode slurries for lithium ion batteries, Ceram. Int. 40 (2014) 4591–4598.
[28] S. Lim, S. Kim, K.H. Ahn, S.J. Lee, The effect of binders on the rheological properties and the microstructure formation of lithium-ion battery anode slurries, J. Power Sources 299 (2015) 221–230.
[29] F. Jeschull, D. Brandell, M. Wohlfahrt Mehrens, M. Memm, Water-soluble binders for lithium-ion battery graphite electrodes: slurry rheology, coating adhesion, and electrochemical performance, Energy Technol. 5 (2017) 2108–2118.
[30] F. Ma, Y. Fu, V. Battaglia, R. Prasher, Microrheological modeling of lithium ion battery anode slurry, J. Power Sources 438 (2019) 226994.
[31] S.H. Sung, S. Kim, J.H. Park, J.D. Park, K.H. Ahn, Role of PVDF in rheology and microstructure of NCM cathode slurries for lithium-ion battery, Materials 13 (20) (2020) 4544.
[32] M. Takeno, T. Fukutsuka, K. Miyazaki, T. Abe, Development of new electronic conductivity measurement method for lithium-ion battery electrode–slurry, Chem. Lett. 46 (2017) 892–894.
[33] M. Takeno, T. Fukutsuka, K. Miyazaki, T. Abe, Influence of carbonaceous materials on electronic conduction in electrode-slurry, Carbon 122 (2017) 202–206.
[34] T. Kusano, M. Ishii, M. Tani, O. Hiruta, T. Matsunaga, H. Nakamura, Rheological behavior of concentrated slurry and wet granules for lithium ion battery electrodes, Adv. Powder Technol. 31 (11) (2020) 4491–4499.
[35] L. Ouyang, Z. Wu, J. Wang, X. Qi, Q. Li, J. Wang, S. Lu, The effect of solid content on the rheological properties and microstructures of a Li-ion battery cathode slurry, RSC Adv. 10 (2020) 19360–19370.
[36] I.M. Krieger, T.J. Dougherty, A mechanism for non-Newtonian flow in suspensions of rigid spheres, Trans. Soc. Rheol. 3 (1959) 137–152.
[37] G. Lutringer, G. Weill, Solution properties of poly(vinylidene fluoride): 1. Macromolecular characterization of soluble samples, Polymer 32 (1991) 877–882.
[38] R.J. Farris, Prediction of the viscosity of multimodal suspensions from unimodal viscosity data, Trans. Soc. Rheol. 12 (1968) 281–301.
[39] J.F. Le Meins, P. Moldenaers, J. Mewis, Suspensions in polymer melts. 1. Effect of particle size on the shear flow behavior, Ind. Eng. Chem. Res. 41 (2002) 6297–6304.